NANOMATERIALS

Shape regulation of high-index facet nanoparticles by dealloying

Liliang Huang[1], Mohan Liu[1], Haixin Lin[2,3], Yaobin Xu[1], Jinsong Wu[1], Vinayak P. Dravid[1,2], Chris Wolverton[1], Chad A. Mirkin[1,2,3]*

Tetrahexahedral particles (~10 to ~500 nanometers) composed of platinum (Pt), palladium, rhodium, nickel, and cobalt, as well as a library of bimetallic compositions, were synthesized on silicon wafers and on catalytic supports by a ligand-free, solid-state reaction that used trace elements [antimony (Sb), bismuth (Bi), lead, or tellurium] to stabilize high-index facets. Both simulation and experiment confirmed that this method stabilized the {210} planes. A study of the PtSb system showed that the tetrahexahedron shape resulted from the evaporative removal of Sb from the initial alloy—a shape-regulating process fundamentally different from solution-phase, ligand-dependent processes. The current density at a fixed potential for the electro-oxidation of formic acid with a commercial Pt/carbon catalyst increased by a factor of 20 after transformation with Bi into tetrahexahedral particles.

The atomic structure of metal nanoparticles (NPs), and of exposed facets in particular, can directly influence catalytic activity (*1*–*3*). Thermolysis of solid-state precursors, a method widely used in industry for producing noble metal NPs at scale (*4*), typically yields thermodynamically favored NPs that have flat low-index facets (*5*) that can have much lower catalytic activity for certain reactions than those with high-index facets with low coordination metal sites. For the latter, only a limited number of methods have been reported for producing them in ligand-free form at scale (*2*, *6*, *7*), and most of these are relatively low-throughput electrochemical methods. Higher-throughput solution-phase methods to control particle shape (*6*, *8*, *9*) typically rely on stabilizing ligands that are often difficult to remove and can adversely affect catalytic activity by blocking active sites (*10*).

Inspired by the observation that underpotential deposition (UPD) of trace amounts of shape-regulating metal elements can be used to synthesize NPs with high-index facets (*8*), we hypothesized that solid-phase syntheses could be used to similarly control anisotropic growth of NPs of metals often used in catalysis with trace amounts of foreign shape-directing elements. We heated solid-state metal precursors of interest in a tube furnace with a foreign metal (Sb, Bi, Pb, and Te) atmosphere to influence NP growth. The foreign metals were chosen on the basis of their low evaporation temperatures and their known ability to promote many catalytic reactions, such as the electro-oxidation of formic acid, a promising alternative fuel for fuel cells (*11*–*18*). Indeed, we show that this strategy can be used to prepare tetrahexahedron (THH)–shaped Pt, Pd, Rh, Ni, Co, and a library of bimetallic NPs, regardless

[1]Department of Materials Science and Engineering, Northwestern University, Evanston, IL 60208, USA. [2]International Institute for Nanotechnology, Northwestern University, Evanston, IL 60208, USA. [3]Department of Chemistry, Northwestern University, Evanston, IL 60208, USA.
*Corresponding author. Email: chadnano@northwestern.edu

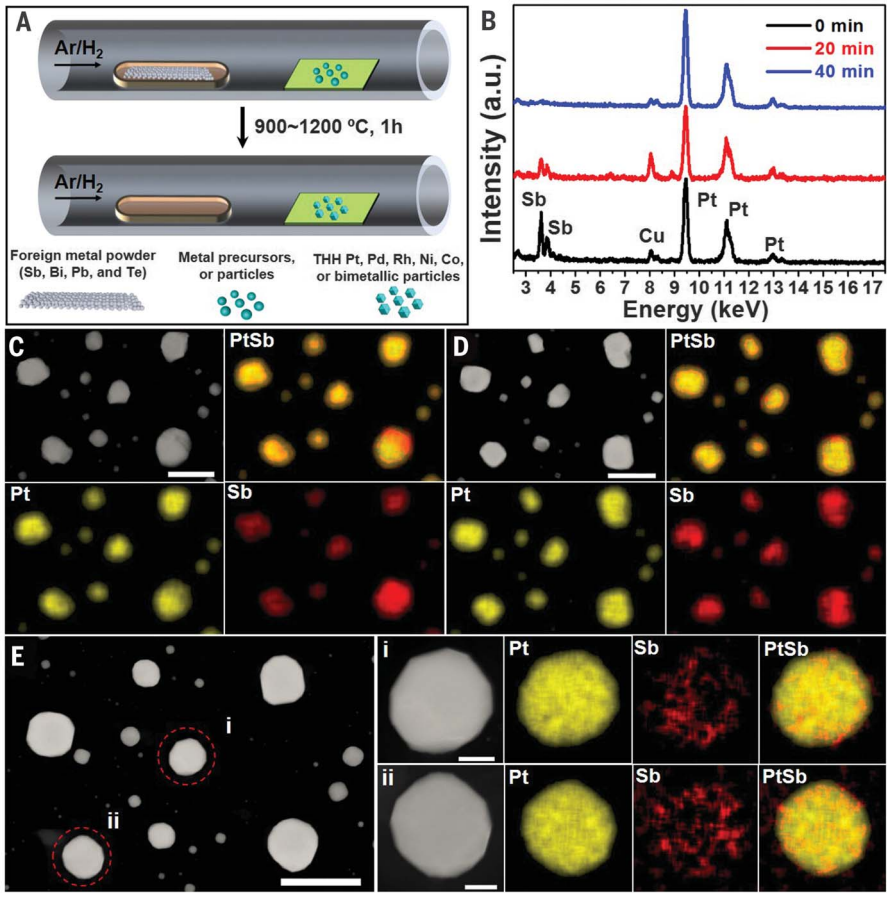

Fig. 1. Synthesizing THH particles through alloying/dealloying with foreign metals (Sb, Bi, Pb, and Te). (**A**) Scheme for synthesizing THH particles with a CVD setup. Approximately 1 mg of the foreign metal powder was loaded in a combustion boat, which was then transferred to a tube furnace. A silicon wafer coated with the metal salt precursors of interest or irregularly shaped particles was placed in the tube, downstream from the foreign metal powder. After thermal treatment in an Ar (or Ar/H_2) atmosphere, the tube was quenched in air and then cooled to room temperature. The foreign metal powder was completely transferred to the silicon wafer with metal precursors via evaporation and THH particles formed. (**B**) EDS spectra of the synthesized particles after reacting at 900°C as a function of time. The Cu signals are from the TEM sample holder. (**C** to **E**) STEM images and EDS elemental maps of the synthesized particles in the same area after reacting at 900°C for 0 min (26.3% Pt, 73.7% Sb) (C), 20 min (37.9% Pt, 62.1% Sb) (D), and 40 min (84.9% Pt, 15.1% Sb) (E). In (E), STEM images and corresponding EDS elemental maps (right) for the particles circled in red provide a clear view of particle morphology and elemental distribution. Scale bars in (i) and (ii), 50 nm; others, 300 nm.

Downloaded from http://science.sciencemag.org/ on September 24, 2019

of foreign metal, after the appropriate thermal treatment. This strategy can be used for bulk-scale synthesis and with control over NP size uniformity. Both density functional theory (DFT) (*19*, *20*) and electron microscopy studies were used to determine why and how this shape-directing process occurs. Finally, Sb-, Bi-, Pb-, and Te-modified THH-shaped Pt NPs were evaluated as electrocatalysts for formic acid oxidation.

In our initial experiments, mixtures of metal precursors of interest and foreign metal powders were heated on a silicon wafer (fig. S1A). Upon reaction completion and subsequent cooling, the morphology of the resulting NPs was confirmed to be THH by scanning electron microscopy (SEM) (fig. S1B). The synthesis was readily scaled to gram quantities (fig. S1, C and D) by replacing the flat wafer with typical catalyst supports with high specific surface areas (such as carbon black) that had strong interactions with the NPs, such that the as-synthesized THH particles were reduced in size from >200 nm to ≤20 nm on average (fig. S1E). Although the THH particles converted directly from metal salt precursors on the silicon wafer were typically polydisperse in size (edge length along [100] direction: 206 ± 144 nm, sample size: 100), monodisperse THH particles (edge length along [100] direction: 63 ± 6.0 nm, sample size: 100) were obtained by using monodisperse cube-shaped NPs (edge length: 46 ± 3.7 nm, sample size: 100) (*21*) as starting materials and then transforming them with the same method into monodisperse THH particles (fig. S1, F to J) (*22*).

To better understand the THH formation process, we used a chemical vapor deposition (CVD) chamber in which the foreign metals were placed upstream of a tube furnace and were carried by argon/hydrogen flow to the metal precursors upon thermal treatment (Fig. 1). The reactor is reminiscent of the vapor-liquid-solid method for the catalytic growth of semiconductor nanowires from metal catalysts (*23*), but here it was used to determine the structural and morphological evolution of Sb-modified Pt THH NPs. The SEM images confirmed the high-yield (1000 out of 1000) formation of THH particles by CVD (Fig. 2, A to E). The dominant exposed facets were high-index {210} planes, which were indexed by transmission electron microscopy (TEM) images and their corresponding selected-area electron diffraction (SAED) patterns. An ideal THH model surrounded by {210} facets correlated well with the TEM-imaged structures. A high-resolution TEM (HRTEM) image of the NPs showed the atomic arrangement of the atoms on the (210) plane, which also correlated well with an atomic model of a (210) facet (Fig. 2, F to J).

Reaction temperature, time, and amount of Sb powder were systematically explored to determine their relative importance (figs. S2 to S7). Higher temperatures led to more rapid THH-shaped NP formation but also to a decreased time window for generating high-quality THH particles. At higher temperatures, Sb dealloying occurred at a faster rate, and a temperature of ≥900°C was required to produce THH-shaped Pt NPs with smooth surfaces. When greater amounts of Sb were used, the formation of the THH shape was delayed because dealloying took longer to finish (fig. S3). Scanning TEM (STEM) and energy-dispersive x-ray spectroscopy (EDS) supported this conclusion (Fig. 1, B to E, and figs. S5 and S6). Specifically, the two techniques showed that THH-shaped Pt NPs formed as the Sb dealloyed from the initial Sb-rich Pt-Sb alloy NPs. This alloying-dealloying shape-regulating process is distinct from the classical additive-growth process that defines conventional wet chemistry methods (*1*, *3*, *6*, *8*–*10*). Finally, if we started with THH NPs and used the same setup to transfer Sb to them, the alloying process created irregularly shaped NPs; this result showed that the Sb dealloying process was critical for generating the near-perfect THH NPs (figs. S8 and S9).

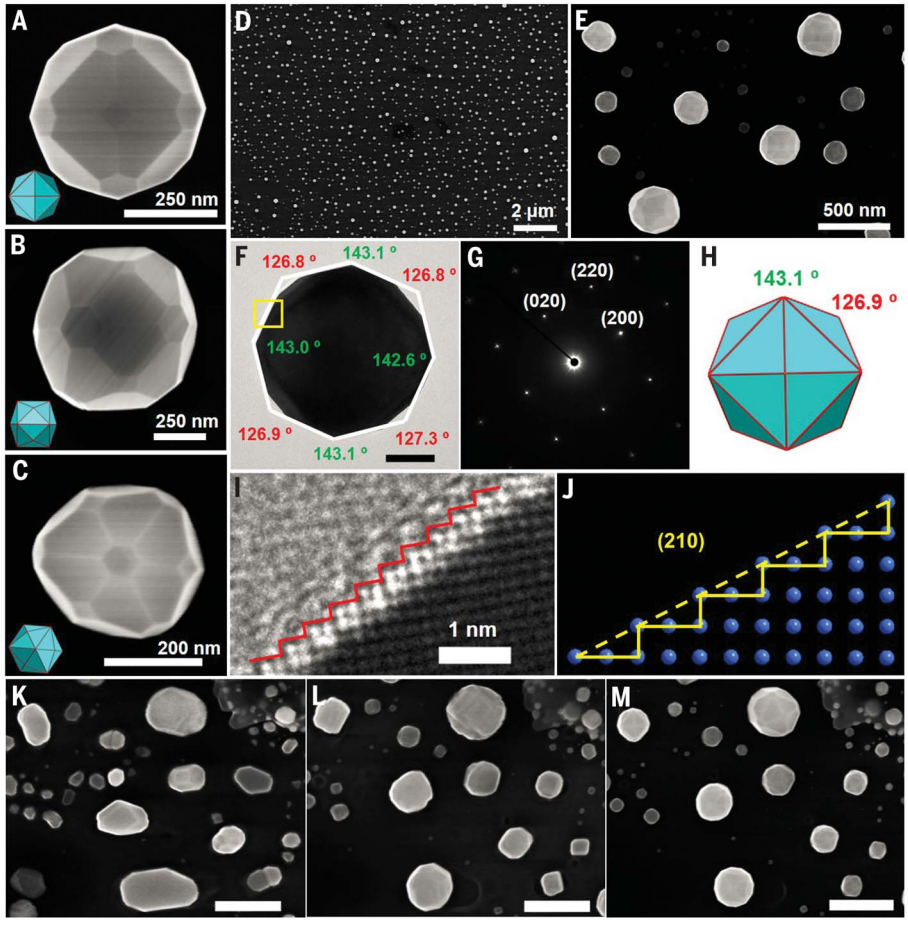

Fig. 2. THH Pt particles synthesized through Sb modification. (**A** to **E**) Representative SEM images of THH Pt particles recorded along the [100], [110], and [111] crystal directions [(A) to (C)], and THH Pt particles dispersed on a silicon wafer [(D) and (E)]. (**F**) TEM image of a THH Pt particle recorded along the [001] direction. White lines are used to highlight the particle facets as a guide to the eye. (**G**) Corresponding diffraction pattern for the particle in (F). (**H**) An ideal model of a THH particle surrounded by {210} facets projected along the [001] direction. A careful measurement of angles between surface planes of the nanoparticle in (F) indicates that the Miller indices of exposed high-index facets are {210}. (**I**) A HRTEM image recorded from the boxed area in (F). Red lines are drawn to highlight the surface (210) plane as a guide to the eye. (**J**) An atomic model of the (210) plane. (**K** to **M**) SEM images of Pt particles synthesized on a silicon wafer by thermally decomposing H_2PtCl_6 at 700°C for 30 min without using Sb powder (K), heating the sample shown in (K) at 900°C for 30 min using 1 mg Sb powder (L), and heating the sample shown in (L) at 900°C for 30 min without using Sb powder (M). Scale bars, 20 nm (F), 300 nm [(K) to (M)].

Because the alloying and dealloying of Pt NPs with Sb vapor both proceeded independently of the initial NP shape, we hypothesized that this strategy could be used as an effective method for recycling ill-shaped Pt waste catalysts, an important industrial concern for the wide-scale application of noble metal catalysts (*24*). To initially test this hypothesis, we synthesized Pt NPs on a silicon wafer by thermally decomposing H_2PtCl_6 at 700°C (Fig. 2K and fig. S10A). The resulting NPs exhibited irregular shapes, similar to the random shapes observed with waste catalysts, thereby establishing a model system for testing the shape-repairing capability of the

Downloaded from http://science.sciencemag.org/ on September 24, 2019

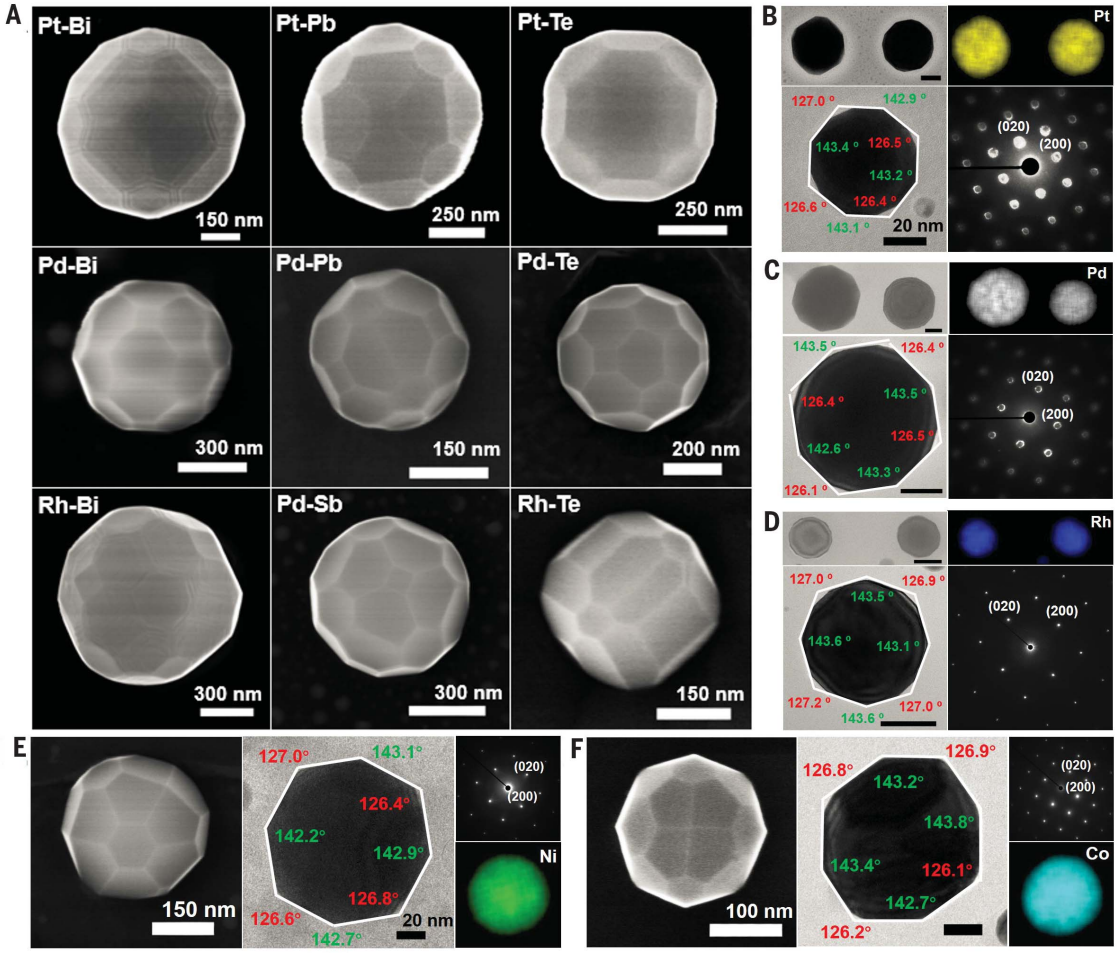

Fig. 3. THH Pt, Pd, Rh, Ni, and Co particles synthesized through foreign metal (Sb, Bi, Pb, and Te) modification. (**A**) SEM images of Pt, Pd, and Rh particles synthesized through Sb, Bi, Pb, and Te modification. (**B** to **D**) STEM images, EDS elemental maps, TEM images, and corresponding diffraction patterns of the Pt-Bi (96.5% Pt, 3.5% Bi) particles (B), Pd-Bi (98.8% Pd, 1.2% Bi) particles (C), and Rh-Bi (99.8% Rh, 0.2% Bi) particles (D). (**E** and **F**) SEM images, TEM images, corresponding diffraction patterns, and EDS elemental maps of the Ni-Bi (99.4% Ni, 0.6% Bi) particles (E) and the Co-Bi (99.6% Co, 0.4% Bi) particles (F). Scale bars, 50 nm unless otherwise noted.

alloying-dealloying process. The sample was then heated to 900°C for 30 min with 1 mg of Sb as the foreign metal source. The resulting Pt-Sb alloy NP exhibited primarily low-index cubic shapes (Fig. 2L and fig. S10B). The Sb source was removed, and the NPs were further heated at 900°C for another 30 min. The SEM images of the resulting NPs (Fig. 2M and fig. S10, C and D) confirmed that >99% of them exhibited a truncated THH morphology, thereby confirming that this method may be useful for reestablishing the catalytically important THH particles from catalysts that have been deactivated (see below).

For the syntheses discussed above, after completion of the heat treatment, the THH NPs were quenched to room temperature by removing the tube containing them from the furnace. If slow cooling was used instead, THH NPs with rough surfaces were obtained, as opposed to the particles with smooth surfaces that resulted from quenching (fig. S11). The smooth surfaces were stabilized with Sb in the high-index planes, and when heated at temperatures below 900°C, they were not stable and restructured into facets with nanoscopic terrace-and-step structures. Indeed, if high-quality THH structures were annealed at 600°C for 12 hours, this process could be visualized by electron microscopy (figs. S12 and S13). The smooth {210} facets could be regenerated by reheating the same particles at 900°C, which initiated the Sb-dealloying process (figs. S11 and S12). This reversible surface reconstruction of the Pt {210} facets, caused by the internal redistribution of Sb, appears to be a previously undiscovered type of shape-recovery process.

In addition to Sb, the trace elements Bi, Pb, and Te could also induce the formation of truncated THH-shaped Pt NPs (Fig. 3A). This strategy proved useful for synthesizing THH-shaped NPs of the noble metals Pd and Rh, as well as Ni and Co, where shape control has not been previously reported (Fig. 3 and fig. S14). The Miller indices of the exposed planes for these particles were confirmed to be {210}, which are the same as those of the Sb-modified THH-shaped Pt NPs. The generalizability of this strategy was further demonstrated by synthesizing a library of bimetallic NPs through Bi modification (Fig. 4 and figs. S14 and S15).

For Pt NPs with a face-centered cubic (fcc) structure, the specific surface energies (on a per-area basis) of the different crystal facets are rank-ordered $\sigma_{(111)} < \sigma_{(100)} < \sigma_{(110)} < \sigma_{(210)}$ (*25*, *26*), and the equilibrium shape for single-crystalline Pt particles is a truncated octahedron (*5*, *27*). The predominant existence of the {210} facets in the synthesized Pt particles indicates that Sb modification stabilizes the {210} facets by reducing their specific surface energy. X-ray diffraction data (fig. S16) showed that the atomic ordering of the Pt and Sb within the NPs cannot be the reason for the formation of the THH-shaped Pt NPs. Indeed, a time-course study shows that the only observed intermetallic-phase (Pt_3Sb) NPs formed at earlier time points do not take on the THH morphology. Only when the vast majority of the Sb was removed (>95%) and the bulk was essentially pure Pt could the THH morphology be observed. Thus, we conclude that the Sb modification in such NPs is primarily on the surface.

To test this hypothesis, we used DFT to calculate the specific surface energies of the (210) plane, the three low-index facets (100), (111), and (110), and different types of high-index planes after Sb modification (figs. S17 to S19 and tables S1 to S4). The computational results confirmed that the specific surface energies of these facets changed drastically after Sb modification, and the specific surface energy of Pt(210)-Sb was the lowest among the considered facets, consistent with the conclusion that Sb on the surface of

Downloaded from http://science.sciencemag.org/ on September 24, 2019

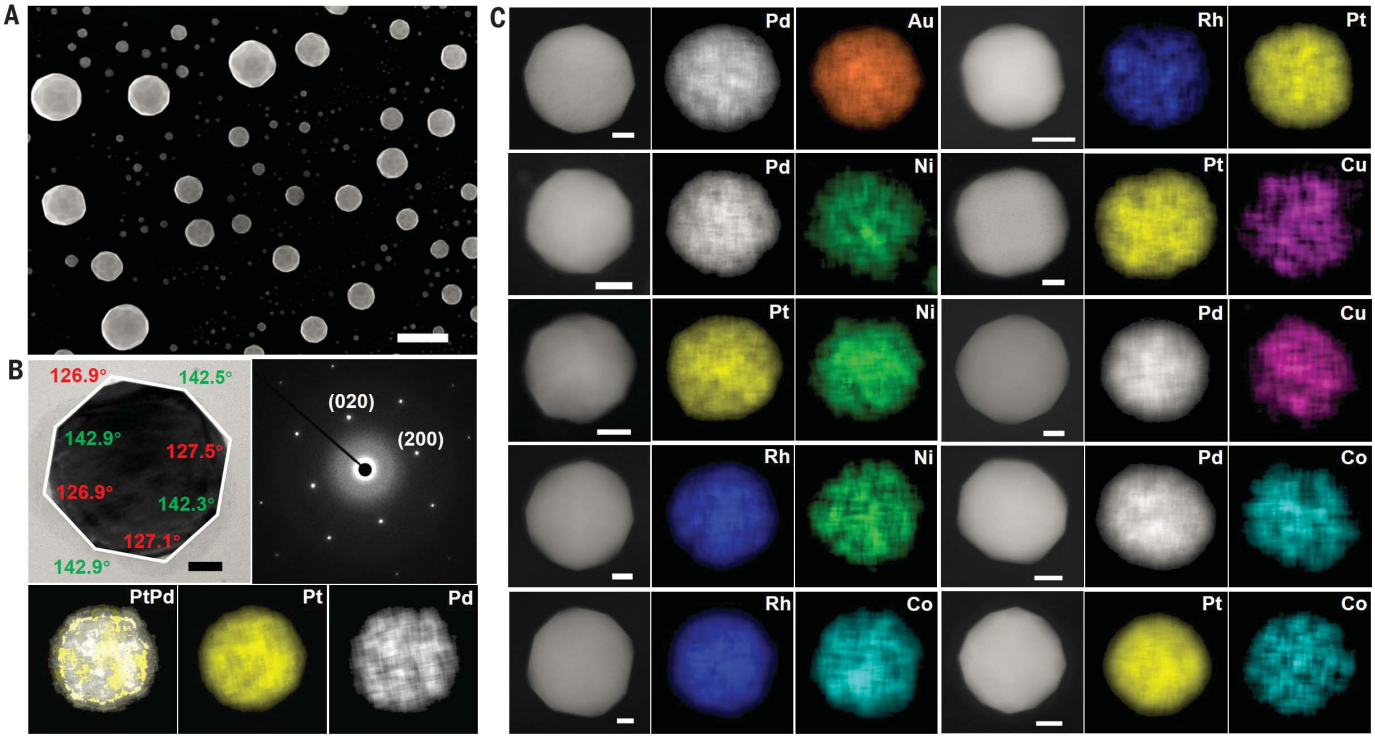

Fig. 4. THH-shaped bimetallic particles synthesized through Bi modification. (**A**) SEM image of THH-shaped PtPd particles synthesized on a silicon wafer. (**B**) TEM image, corresponding diffraction pattern, and EDS elemental maps for a THH-shaped PtPd-Bi (18.1% Pt, 81.7% Pd, 0.2% Bi) particle. (**C**) STEM images (columns 1 and 4) and EDS elemental maps (columns 2, 3, 5, and 6) for THH-shaped PdAu-Bi (89.3% Pd, 10.6% Au, 0.1% Bi), RhPt-Bi (82.1% Rh, 17.6% Pt, 0.3% Bi), PdNi-Bi (57.3% Pd, 41.1% Ni, 1.6% Bi), PtCu-Bi (88.5% Pt, 11.4% Cu, 0.1% Bi), PtNi-Bi (55.1% Pt, 44.5% Ni, 0.4% Bi), PdCu-Bi (77.6% Pd, 22.1% Cu, 0.3% Bi), RhNi-Bi (74.8% Rh, 25.1% Ni, 0.1% Bi), PdCo-Bi (70.7% Pd, 29.1% Co, 0.2% Bi), RhCo-Bi (66.5% Rh, 33.4% Co, 0.1% Bi), and PtCo-Bi (78.4% Pt, 21.1% Co, 0.5% Bi) particles. Scale bars, 500 nm (A), 20 nm [(B) and (C)].

NPs plays a central role in stabilizing the THH morphology.

The elements Sb, Bi, Pb, and Te are favorable for promoting the catalysts' efficiency and stability toward the electro-oxidation of formic acid (*11*–*18*), an attractive choice for chemical fuels in fuel cells (*28*, *29*). Furthermore, {210} facets possess the highest density of step atoms in the [001] zone and are the most "open" planes of an fcc crystal (*7*, *30*). Finally, Pt NPs with {210} facets have been reported to exhibit extremely high catalytic activity for formic acid electro-oxidation (*31*). We studied the catalytic activities of bulk-scale synthesized Pt-M (M = Sb, Bi, Pb, Te) and Pd-Bi THH NPs on carbon black toward formic acid electro-oxidation, and confirmed that they are catalytically more active than commercial Pt/C and Pd/C catalysts (fig. S1, C to E, and figs. S20 to S26). The current density of the THH Pt particles made from a commercial Pt/C catalyst (Pt/C-Bi THH, 1.37 A/mg) is 20 times that of the as-purchased catalyst (0.07 A/mg) at an overpotential of 0.5 V (fig. S26, A and B).

Unlike conventional synthesis methods for NPs with high-index facets, this strategy is remarkably easy to use, scalable, and effective for industrial production. Additionally, because deactivated structures that have lost their high-index facets can be recycled, it may be particularly attractive for catalyst recovery and reactivation processes that we have further investigated and characterized with a commercial catalyst sample (fig. S27). To fully take advantage of this new methodology, we and others need to explore and define the limits of size control, the atom-level mechanism of shape control, and the role of support interactions.

REFERENCES AND NOTES

1. H. Lee *et al.*, *Angew. Chem. Int. Ed.* **45**, 7824–7828 (2006).
2. N. Tian, Z. Y. Zhou, S. G. Sun, Y. Ding, Z. L. Wang, *Science* **316**, 732–735 (2007).
3. M. Grzelczak, J. Pérez-Juste, P. Mulvaney, L. M. Liz-Marzán, *Chem. Soc. Rev.* **37**, 1783–1791 (2008).
4. M. V. Twigg, in *Catalyst Handbook* (CRC Press, 1989), pp. 34–43.
5. A. S. Barnard, N. P. Young, A. I. Kirkland, M. A. van Huis, H. Xu, *ACS Nano* **3**, 1431–1436 (2009).
6. J. Zhang, Q. Kuang, Y. Jiang, Z. Xie, *Nano Today* **11**, 661–677 (2016).
7. N. Tian, Z. Y. Zhou, S. G. Sun, *J. Phys. Chem. C* **112**, 19801–19817 (2008).
8. M. L. Personick, M. R. Langille, J. Zhang, C. A. Mirkin, *Nano Lett.* **11**, 3394–3398 (2011).
9. C. Burda, X. Chen, R. Narayanan, M. A. El-Sayed, *Chem. Rev.* **105**, 1025–1102 (2005).
10. Z. Niu, Y. Li, *Chem. Mater.* **26**, 72–83 (2013).
11. L. An *et al.*, *Nano Energy* **15**, 24–32 (2015).
12. Y. Kang *et al.*, *ACS Nano* **6**, 2818–2825 (2012).
13. Q. S. Chen *et al.*, *J. Am. Chem. Soc.* **133**, 12930–12933 (2011).
14. X. Yu, P. G. Pickup, *Electrochim. Acta* **55**, 7354–7361 (2010).
15. J. K. Lee, H. Jeon, S. Uhm, J. Lee, *Electrochim. Acta* **53**, 6089–6092 (2008).
16. S. Uhm, S. T. Chung, J. Lee, *Electrochem. Commun.* **9**, 2027–2031 (2007).
17. E. Herrero, M. Llorca, J. Feliu, A. Aldaz, *J. Electroanal. Chem.* **394**, 161–167 (1995).
18. J. Clavilier, A. Fernandez-Vega, J. Feliu, A. Aldaz, *J. Electroanal. Chem.* **258**, 89–100 (1989).
19. G. Kresse, J. Furthmüller, *Phys. Rev. B* **54**, 11169–11186 (1996).
20. G. Kresse, J. Furthmüller, *Comput. Mater. Sci.* **6**, 15–50 (1996).
21. W. Niu *et al.*, *Cryst. Growth Des.* **8**, 4440–4444 (2008).
22. See supplementary materials.
23. Y. Xia *et al.*, *Adv. Mater.* **15**, 353–389 (2003).
24. K. Morgan, A. Goguet, C. Hardacre, *ACS Catal.* **5**, 3430–3445 (2015).
25. J. M. Zhang, F. Ma, K. W. Xu, *Appl. Surf. Sci.* **229**, 34–42 (2004).
26. Y. N. Wen, J. M. Zhang, *Solid State Commun.* **144**, 163–167 (2007).
27. T. Avanesian *et al.*, *J. Am. Chem. Soc.* **139**, 4551–4558 (2017).
28. S. Ha, R. Larsen, R. I. Masel, *J. Power Sources* **144**, 28–34 (2005).
29. X. Yu, P. G. Pickup, *J. Power Sources* **182**, 124–132 (2008).
30. D. Löffler, L. Schmidt, *Surf. Sci.* **59**, 195–204 (1976).
31. S. G. Sun, Y. Lin, N. H. Li, J. Q. Mu, *J. Electroanal. Chem.* **370**, 273–280 (1994).

ACKNOWLEDGMENTS

We thank Y. Kang for helpful discussion on electrochemistry.
Funding: Supported by the Sherman Fairchild Foundation Inc.

Downloaded from http://science.sciencemag.org/ on September 24, 2019

(synthesis and characterization of monometallic particles), the Center for Bio-Inspired Energy Science, an Energy Frontier Research Center funded by the U.S. Department of Energy, Office of Science, Basic Energy Sciences under award DE-SC0000989 (synthesis of electrocatalysts), and Kairos Ventures (synthesis and characterization of bimetallic nanoparticles). M.L. and C.W. acknowledge support from the Toyota Research Institute. This project made use of the EPIC facility of Northwestern University's NUANCE Center, which has received support from the Soft and Hybrid Nanotechnology Experimental (SHyNE) Resource (NSF ECCS-1542205); the MRSEC program (NSF DMR-1720139) at the Materials Research Center; the International Institute for Nanotechnology (IIN); the Keck Foundation; and the State of Illinois, through the IIN. This project made use of the J. B. Cohen X-Ray Diffraction Facility supported by MRSEC and SHyNE. This project made use of resources in National Energy Research Scientific Computing Center and Northwestern University's Quest high-performance computing system. **Author contributions:** L.H., H.L., and C.A.M. conceived the idea and designed the experiments; L.H. carried out experiments on nanocatalyst synthesis, characterization, and electrocatalytic performance tests; L.H. and H.L. analyzed the data; M.L. and C.W. performed DFT studies; Y.X., J.W., and V.P.D. performed TEM characterization; C.A.M., C.W., and V.P.D. supervised the project; and L.H., M.L., H.L., and C.A.M. wrote the paper. **Competing interests:** U.S. patent application 62/712,416 has been filed on this work. **Data and materials availability:** All data are available in the manuscript or the supplementary materials.

SUPPLEMENTARY MATERIALS

science.sciencemag.org/content/365/6458/1159/suppl/DC1
Materials and Methods
Figs. S1 to S27
Tables S1 to S4
References (*32*–*43*)

4 April 2019; accepted 13 August 2019
10.1126/science.aax5843

Downloaded from http://science.sciencemag.org/ on September 24, 2019

Science

Shape regulation of high-index facet nanoparticles by dealloying

Liliang Huang, Mohan Liu, Haixin Lin, Yaobin Xu, Jinsong Wu, Vinayak P. Dravid, Chris Wolverton and Chad A. Mirkin

Science **365** (6458), 1159-1163.
DOI: 10.1126/science.aax5843

Stabilizing rougher nanoparticles

For many reactions catalyzed by metal nanoparticles, the more exposed metal atoms on high-index faces can be more active than metal atoms on smooth, low-index faces. Surface ligands can be used to stabilize high-index surfaces, but they can also be hard to remove. Huang *et al.* report the solid-state synthesis of metal nanoparticles such as platinum and chromium that can form tetrahexahedral nanoparticles with high-index faces. Metals such as bismuth and lead were alloyed with the transition metals at high temperatures and then evaporatively dealloyed during a quench to room temperature.

Science, this issue p. 1159

ARTICLE TOOLS http://science.sciencemag.org/content/365/6458/1159

SUPPLEMENTARY MATERIALS http://science.sciencemag.org/content/suppl/2019/09/11/365.6458.1159.DC1

REFERENCES This article cites 42 articles, 2 of which you can access for free
http://science.sciencemag.org/content/365/6458/1159#BIBL

PERMISSIONS http://www.sciencemag.org/help/reprints-and-permissions

Use of this article is subject to the Terms of Service

Science (print ISSN 0036-8075; online ISSN 1095-9203) is published by the American Association for the Advancement of Science, 1200 New York Avenue NW, Washington, DC 20005. The title *Science* is a registered trademark of AAAS.

Copyright © 2019 The Authors, some rights reserved; exclusive licensee American Association for the Advancement of Science. No claim to original U.S. Government Works

Downloaded from http://science.sciencemag.org/ on September 24, 2019